Online Grid Impedance Estimation for Enhancing the Stability of Type IV Wind Turbines Connected to Weak networks

Mohammed Y. Morgan, Amgad A. El-Deib and Magdy El-Marsafawy, *Member, IEEE*

Abstract:Large scale integration of wind power is one of the main challenges in today power systems. Large off -shore wind farms are usually connected to grids through long transmission lines or cables. These weak grid conditions have great influence on the stability of wind power plant's operation. This paper analyses the stability issues raised by integrating wind farms into ac network with very weak conditions .The paper also proposes a gain schedule based adaptive controller for the grid side converter to enhance the power system stability at the point of connection. In order to identify the weakness level of the grid to generate the appropriate stabilizing control action an online grid impedance estimation scheme is introduced. The scheme depends on the Extended Kalman-Filter (EKF) to estimate the equivalent grid impedance without the need of active disturbance injection. Using the proposed control scheme the system can operate under very weak grid conditions with higher wind power penetration levels. Simulations under low short circuit ratios are conducted to show the enhanced system stability using the proposed approach.

Key words : Wind Farm, PMSG, VSC, Adaptive, Weak Grid, Kalman Filter.

I. INTRODUCTION

One of the challenges that face the bulk integration of wind energy is weak network connections [1] .Large wind power plants are usually connected to the grid through long transmission lines or cables which results in weak grid connections at the point of common coupling (PCC). Grid strength can change considerably during operation in case of faults, lines tripping or load variations. Consequently, limitations on power injection are imposed. In literature many studies were conducted to enhance the wind power plant stability under weak grid conditions. In [2, 3] an adaptive (gain scheduling) control strategy was adopted by adjusting the voltage controller gain to enhance the system stability under weak grid conditions. Online grid impedance estimation was introduced in [4] using active, reactive power and voltage measurements. This impedance estimation technique was used along with adaptive gain scheduling to enhance the grid side converter stability.

Many studies were also conducted to estimate the grid impedance using power converters online. In these studies, the three main methods are passive, active and quasi- passive. Passive methods [5] use the existing disturbances in the power networks to the grid impedance at the fundamental or low order harmonic frequencies. Active methods [6] force a disturbance into the grid using the power converter without affecting the normal operation to determine the grid impedance. Quasi passive methods [7] use hybrid identification techniques to determine the impedance by changing the power converter operation point. In [8], a new parameter estimation method that is based on EKF is presented to estimate the grid impedance which can be used in addition to the control of grid connected converters.

The objective of this paper is to introduce an adaptive controller to help damping the oscillations resulting from the weak grid interconnection. EKF based online grid impedance estimation is introduced to provide the controller with the grid weakness level. Accordingly the controller will generate the required adaptive control signal to ensure system stability under very weak grid conditions. The paper is organized as follows: A PMSG wind turbine generator small signal model developed using MATLAB Linear Analysis tool is introduced in Section II. The model is then validated against time domain simulations adopted by MATLAB/Simulink. A system stability study using Modal analysis under low short circuit ratios (SCRs) is presented in Section III. Grid impedance estimation using EKF and the proposed adaptive control scheme are introduced in Section IV. Finally the simulation results are introduced in Section V.

II. TEST SYSTEM MODELING

A schematic of the wind turbine model is shown in Fig.1. The model consists of a variable-speed wind turbine directly driving a 1.5 MW permanent magnet synchronous generator (PMSG). The PMSG converter is connected to the PCC through step-up unit transformer (0.69/33 kV) connected to collector system and followed by the main transformer (33/230 kV).

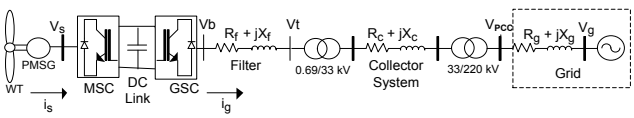

Fig. 1. PMSG wind turbine test system model.

A. Drive Train Model (Two-mass Model)

The drive train model introduces wind turbine mechanical dynamics. In this model we will use the two mass model [9]. The linearized model, is given by

$$\Delta\dot{\theta}_{tr} = \omega_b(\Delta\omega_t - \Delta\omega_r) \quad (1)$$

$$\Delta\dot{\omega}_t = \frac{1}{2H_t}(\Delta T_m - K_{tr}\Delta\theta_{tr} - D_{tr}(\Delta\omega_t - \Delta\omega_r) - D_t\Delta\omega_t) \quad (2)$$

$$\Delta\dot{\omega}_r = \frac{1}{2H_r}(K_{tr}\theta_{tr} - D_{tr}(\Delta\omega_r - \Delta\omega_t) - D_r\Delta\omega_r - \Delta T_e) \quad (3)$$

$$\Delta T_m = \frac{3C_p v_{wo}^2}{\omega_{to}}\Delta v_w - \frac{C_p v_{wo}^3}{\omega_{to}^2}\Delta\omega_t \quad (4)$$

where θ_{tr} is the shaft twist angle; ω_t , ω_r and ω_b is the wind turbine , generator rotor and base angular speeds respectively; H_t , H_r and K_{tr} are the wind turbine / PMSG inertia constant and shaft stiffness respectively; D_t , D_r and D_{tr} are the wind turbine, rotor and mutual damping coefficient respectively; T_m is the input mechanical torque; ρ is the air density; R is the turbine blade length; Cp is the performance coefficient; ω_t is the wind turbine speed and v_w is the wind velocity and $T_e$is the electromagnetic torque.

B. Permanent Magnet Synchronous Generator Model

The PMSG Model in p.u. based on the generator convention [9,10], are given by

$$\dot{\iota_{sd}} = \frac{\omega_b}{L_d}(-v_{sd} - R_s i_{sd} + L_q\omega_r i_{sq}) \quad (5)$$

$$\dot{\iota_{sq}} = \frac{\omega_b}{L_q}(-v_{sq} - R_s i_{sq} - L_d\omega_r i_{sd} + \psi_r\omega_r) \quad (6)$$

$$T_e = (\psi_r i_{sq} + (L_d - L_q)i_{sq}i_{sd}) \quad (7)$$

where L_d and L_q are the direct and quadrature axis inductances; i_{sd} and i_{sq} are stator direct and quadrature axis current respectively; v_{sd} and v_{sq} are stator direct and quadrature axis voltage respectively; ψ_r and ω_b are the rotor flux linkages and base angular speed . The linearized model in p.u. , is given by

$$\Delta\dot{\iota_{sd}} = \frac{\omega_b}{L_d}(-\Delta v_{sd} - R_s\Delta i_{sd} + L_q(\omega_{ro}\Delta i_{sq} + i_{sqo}\Delta\omega_r)) \quad (8)$$

$$\Delta\dot{\iota_{sq}} = \frac{\omega_b}{L_q}(-\Delta v_{sq} - R_s\Delta i_{sq} - L_{d(}\omega_{ro}\Delta i_{sd} + i_{sdo}\Delta\omega_r) + \psi_r\Delta\omega_r) \quad (9)$$

$$\Delta T_e = (\psi_r\Delta i_{sq} + (L_d - L_q)(i_{sqo}\Delta i_{sd} + i_{sdo}\Delta i_{sq})) \quad (10)$$

C. Machine Side Converter (MSC) Model

The Machine side converter shown in Fig. 2 includes two control loops .the first loop controls the rotor speed in order to continually maximize wind energy captured by the wind turbine. The rotor speed reference corresponding to maximum power point tracking (MPPT) , derived from the following relationship [11]

$$\omega_{ref} = \frac{v_w\,\lambda_{opt}}{R} \quad (11)$$

where λ_{opt} is the optimal TSR at which the power generated from the wind turbine is maximum. The linearized model in p.u. , is given by

$$\Delta\dot{\varphi}_1 = \Delta\omega_{ref} - \Delta\omega_r \quad (12)$$

$$\Delta\dot{\varphi}_2 = (\Delta i_{sq\,ref} - \Delta i_{sq}) = (k_{p1}\Delta\dot{\varphi}_1 + k_{I1}\Delta\varphi_1) - \Delta i_{sq} \quad (13)$$

$$\Delta v_{sq} = \psi_r\Delta\omega_r - L_d(\omega_{ro}\Delta i_{sd} + i_{sdo}\Delta\omega_r) - (k_{p2}\Delta\dot{\varphi}_2 + k_{I2}\Delta\varphi_2) \quad (14)$$

$$\Delta\dot{\varphi}_3 = (\Delta i_{sd\,ref} - \Delta i_{sd}) = -\Delta i_{sd} \quad (15)$$

$$\Delta v_{sd} = L_q(\omega_{ro}\Delta i_{sq} + i_{sqo}\Delta\omega_r) - (k_{p3}\Delta\dot{\varphi}_3 + k_{I3}\,\Delta\varphi_3) \quad (16)$$

where K_{p1}, K_{i1}, K_{p2}, K_{i2}, K_{p3} and K_{i3} are the gains of the PI controllers; φ_1, φ_2 and φ_3 are the intermediate variables; and $\omega_{r\,ref}$ and $i_{sd\,ref}$ are the reference values for rotor speed and direct access current , respectively.

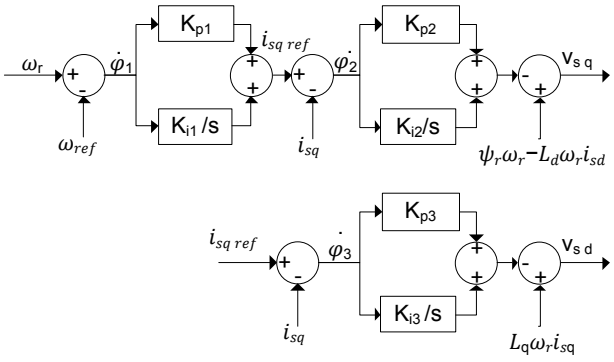

Fig. 2. Machine side converter block diagram.

D. Grid Side Converter (GSC) Model

The GSC shown in Fig. 3 includes two cascaded control loops. The first control loop is used to ensure constant DC-Link voltage for proper operation of the back to back converter [11,12]. The second control loop is used to control the voltage at the point of common coupling by adjusting the reactive power exchanged with the grid.

$$\Delta\dot{\varphi}_4 = \Delta v_{dc\,ref} - \Delta v_{dc} \quad (17)$$

$$\Delta\dot{\varphi}_5 = (k_{p4}\Delta\dot{\varphi}_4 + k_{I4}\Delta\varphi_4) - \Delta i_{gd} \quad (18)$$

$$\Delta v_{bd} = \Delta v_{td} - x_f\Delta i_{gq} - (k_{p5}\Delta\dot{\varphi}_5 + k_{I5}\Delta\varphi_5) \quad (19)$$

$$\Delta\dot{\varphi}_6 = (\Delta v_{\mathrm{pcc\,ref}} - \Delta v_{\mathrm{pcc}}) \quad (20)$$

$$\Delta\dot{\varphi}_7 = (k_{p6}\Delta\dot{\varphi}_6 + k_{I6}\Delta\varphi_6) - \Delta i_{gq} \quad (21)$$

$$\Delta v_{bq} = \Delta v_{tq} + x_f\,\Delta i_{gd} - (k_{p7}\Delta\dot{\varphi}_7 + k_{I7}\Delta\varphi_7) \quad (22)$$

$$\Delta\dot{i}_{gd} = \frac{\omega_b}{L_f}(\Delta v_{bd} - \Delta v_{td} - R_f \Delta i_{gd} + x_f \Delta i_{gq}) \quad (23)$$

$$\Delta\dot{i}_{gq} = \frac{\omega_b}{L_f}(\Delta v_{bq} - \Delta v_{tq} - R_f \Delta i_{gq} - x_f \Delta i_{gd}) \quad (24)$$

where L_f and R_f are the GSC RL filter values. K_{p4}, K_{i4}, K_{p5}, K_{i5}, K_{p6} and K_{i6} are the gains of the PI controllers; φ_4, φ_5 , φ_6 and φ_7 are the intermediate variables; v_{bd} and v_{bq} are GSC output voltage direct and quadrature axis components; v_{td} and v_{tq} are the WT terminal voltage direct and quadrature axis components; and $v_{dc\,ref}$ and Q_{ref} are the reference values for dc link voltage and reactive power delivered to the grid, respectively.

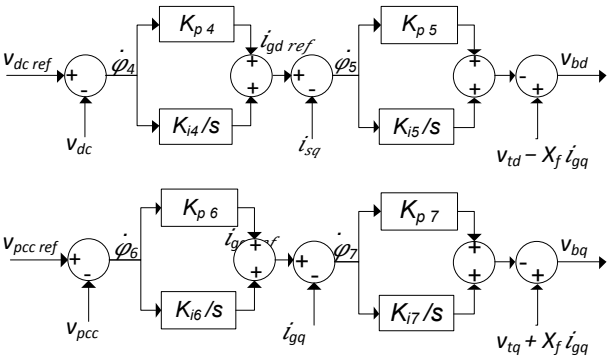

Fig. 3. Grid side converter block diagram.

E. DC link Model

The machine and grid side converters exchange power via the dc link [12]. The power balance equation of DC-Link in p.u. , is given by

$$\dot{v_{dc}} = \frac{\omega_b}{c\, v_{dc}}(P_M - P_G) \quad (25)$$

$$\dot{v_{dc}} = \frac{\omega_b}{c\, v_{dc}}\Big(\big(v_{sd} i_{sd} + v_{sq} i_{sq}\big) - \big(v_{bd} i_{gd} + v_{bq} i_{gq}\big)\Big) \quad (26)$$

The linearized model in p.u. is given by:

$$\Delta\dot{v_{dc}} = \frac{\omega_b}{c\, v_{dco}}\big((v_{sdo}\Delta i_{sd} + v_{sdo}\Delta i_{sd} + v_{sqo}\Delta i_{sq} + v_{sqo}\Delta i_{sq}) - \big(v_{bdo}\Delta i_{gd} + v_{bdo}\Delta i_{gd} + v_{bqo}\Delta i_{gq} + v_{bqo}\Delta i_{gq}\big)\big) \quad (27)$$

where P_M and P_G are the input power from PMSG and the output power to the grid ; v_{dc} and c are the dc link voltage and capacitance, respectively

F. Phase Locked Loop (PLL)

Phase Locked Loop (PLL) synchronization is essential for proper operation of grid side converters (GSC) [11]. The main function of the PLL is to track the ac-grid voltage and obtain its relevant angle in order to synchronize the GSC currents and voltages with the grid frame. The block diagram that illustrates the operation of the PLL is shown in Fig. 4.

$$\dot{\theta_{PLL}} = \omega_o + G_{PLL} v_{tq} \quad (28)$$

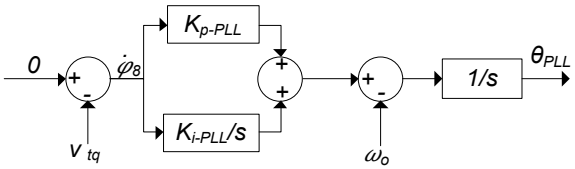

Fig. 4. Phase locked loop (PLL) block diagram.

The linearized model in p.u. , is given by

$$G_{PLL} = k_{P-PLL} + k_{I-PLL}/s \quad (29)$$

$$\Delta\dot{\theta} = (k_{P-PLL}\Delta\dot{\varphi}_7 + k_{I-PLL}\Delta\varphi_7) \quad (30)$$

$$\Delta\dot{\varphi}_8 = -\Delta v_{bq} \quad (31)$$

where $K_{P-\mathrm{PLL}}$and $K_{I-\mathrm{PLL}}$ are the constants of the PI controllers; φ_8 are the intermediate variable; and θ , v_{bq} are the PLL angle and q-component of the wind turbine terminal voltage, respectively.

The generated angle from the PLL is used for transforming voltage and currents between the grid reference frame and the GSC reference frame, as

$$\begin{bmatrix} v_d' \\ v_q' \end{bmatrix} = \begin{bmatrix} \cos\theta & -\sin\theta \\ \sin\theta & \cos\theta \end{bmatrix} \begin{bmatrix} v_d \\ v_q \end{bmatrix} \quad (32)$$

$$\begin{bmatrix} i_d \\ i_q \end{bmatrix} = \begin{bmatrix} \cos\theta & \sin\theta \\ -\sin\theta & \cos\theta \end{bmatrix} \begin{bmatrix} i_d' \\ i_q' \end{bmatrix} \quad (33)$$

where v_{dq}' and i_{dq}' are the currents and voltages in GSC frame and v_{dq} and i_{dq} are the currents and voltages in grid reference frame, respectively.

G. The collector system and grid model

The grid and collector system including the unit and main transformers are modeled in p.u., as

$$\Delta v_{td} = -\frac{L_{eq} + L_g}{\omega_b}\Delta\dot{i}_{gd} + \Delta v_{gd} + \big(R_{eq} + R_g\big)\Delta i_{gd} + (X_{eq} + X_g)\Delta i_{gq} \quad (34)$$

$$\Delta v_{tq} = -\frac{L_{eq} + L_g}{\omega_b}\Delta\dot{i}_{gq} + \Delta v_{gq} + \big(R_{eq} + R_g\big)\Delta i_{gq} + (X_{eq} + X_g)\Delta i_{gd} \quad (35)$$

where L_{eq} , R_{eq} are the equivalent impedance of the collector and transformers ; L_g, R_g are the grid impedance; ; v_{gd} , v_{gq} are the d and q-component of the grid voltage, respectively.

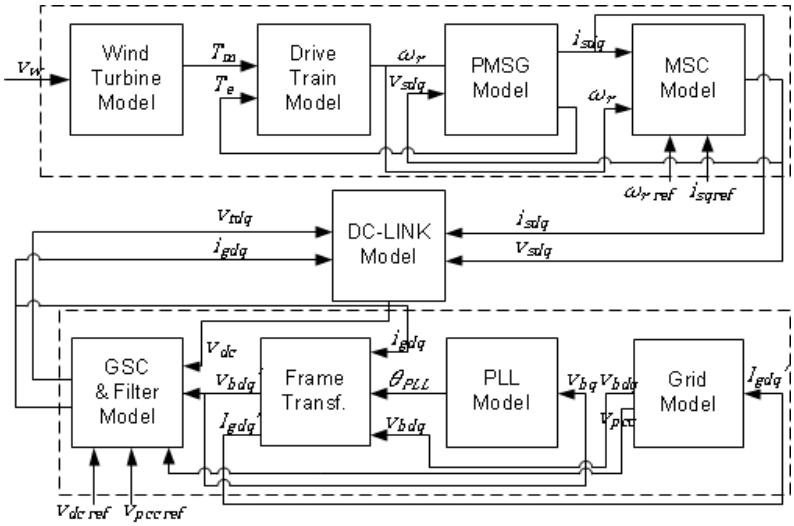

Fig. 5.Test model block diagram

H. *The overall system linearized model*

The total system model is obtained by linking the mechanical system, PMSG, MSC, DC-Link, GSC, PLL, transformer and grid models corresponding equations [13]. The complete system diagram is shown in Fig. 5 which illustrates the link between the various subsystems. The complete system state space model consists of 16 states and, can be written as

$$\Delta\dot{x} = A\,\Delta x + B\,\Delta u \tag{36}$$

where the A is the state matrix, B is the input matrix, x is the state vector and u is the input vector. The state and input vectors, are given as

$$x = [\theta_{tr}\ \omega_t\ \omega_r\ i_{sd}\ i_{sq}\ \varphi_1\ \varphi_2\ \varphi_3\ i_{gd}\ i_{gq}\ \varphi_4\ \varphi_5\ \varphi_6\ v_{dc}\ \theta_{PLL}\ \varphi_7]^T \tag{37}$$

$$u = [v_w\ \ \omega_{r\,ref}\ \ i_{sd\,ref}\ \ v_{dc\,ref}\ \ Q_{\text{ref}}]^T \tag{38}$$

I. *Linearized Model Validation*

In order to validate the small signal model of the test system, all the system dynamics (slow and fast) are to be tested. The slow dynamics of the system are the mechanical system dynamics including the turbine and drive train. The fast dynamics represents the electrical system dynamics including the dc link voltage, PLL, machine side and grids side currents.

Fig. 6 shows the comparison between the linear small-signal model and detailed nonlinear simulation using Simulink following a step down in wind speed from 12 m/s to 11 m/s at (t=1s) and then step up to 12 m/s again at (t=11s) . The comparison shows how the slow dynamics of the system are accurately modeled using the linearized model including the controller's actions. For the sake of model validation for fast dynamics, another comparison between the linearized model and detailed model are shown in Fig. 7.The system is subjected to step up in dc-link voltage reference by 0.05 kV at (t=0.05s) and a step down by 0.1 kV at (t=0.15s). It can be shown that the linearized model provides good accuracy .

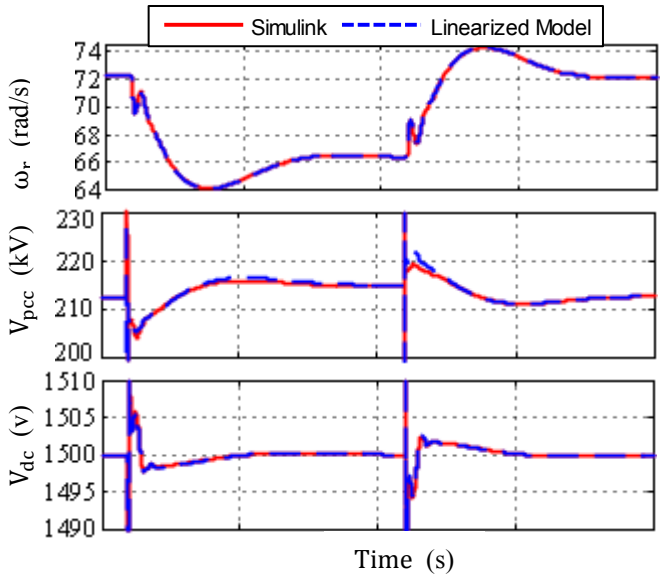

Fig. 6. Linearized model validation for slow dynamics.

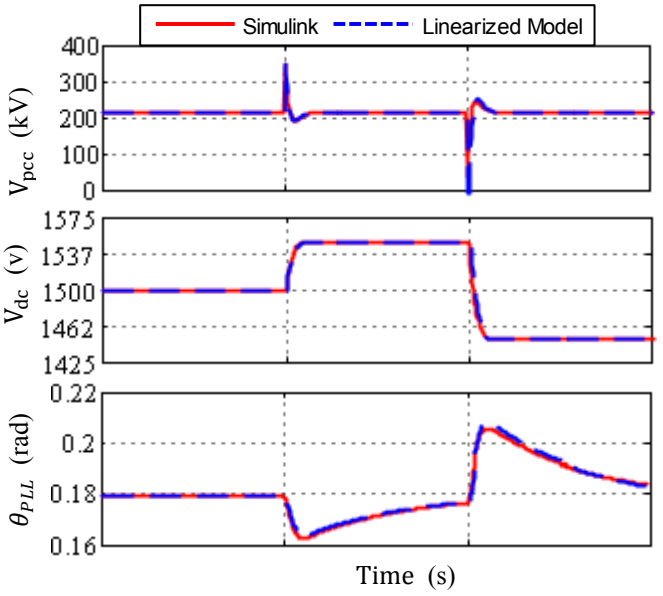

Fig. 7. Linearized model validation for fast dynamics. .

III. Modal Analysis

The proposed system dynamics can be studied with eigenvalue analysis, which is a widely used technique for power system dynamic analysis. The eigenvalue analysis is a great tool for determining the system stability and identifying the poorly damped modes. In order to make the connection between each mode and the system states the relative participation factors of the state variables in the modes can be utilized.

A. Eigenvalue Analysis

Considering the proposed model, the following operating conditions are given as follows: The model is subjected to wind speed of (10 m/s). The voltage control loop is adjusted to maintain PCC voltage at 1 p.u .Considering the grid impedance corresponding to SCR=10, Table I shows the system modes calculated under the previous conditions.

TABLE I

System modes

Mode	Eigenvalue	Oscillation Frequency (Hz)	Damping Ratio (%)
1	-52 ± 333i	53	0.155
2	-300	-	-
3	-245	-	-
4	-127	-	-
5	-134	-	-
6	-20 ± 24i	3.9	0.633
7	-9	-	-
8	-6 ± 24i	3.8	0.234
9	-11 ± 20i	3.2	0.477
10	-5 ± 10i	1.66	0.459
11	-1 ± 1i	0.11	0.646

Table I shows that the system contains 6 pair of complex Eigenvalues corresponding to 6 oscillatory modes and 5 real eigenvalues representing 5 damped modes. The oscillation frequency and the damping ratio for each mode are given in Table I. Participation factors provide connection between system states and oscillatory modes in order to give deep system insights. The system relative participations are shown in Table II which reveals that oscillatory modes (1,6) are associated with GSC control loops especially DC-Link control loop and inner direct axis current control loops. Oscillatory modes (8-11) are clearly associated with Drive Train, PMSG and MSC states but not affected by GSC states.

B. Influence of grid strength reduction

In this section the impact of grid strength reduction on the system stability is investigated. Grid impedance can be represented by short circuit ratio (SCR) which is the ratio between the short circuit power at the PCC and the maximum power injected from the wind turbine [2]. In this paper the SCR for strong grid is considered between 10 to 2 and below 2 the grid is considered weak. In order to investigate the system stability under low grid strength, the SCR is varied from 10 to 1. The modes loci of the small signal model are shown in Fig. 8 where the (SCR=10) operating point is marked by a circle (o) and the (SCR=1) marked by diamond (◊).As shown in Fig. 8 the system eigenvalues sensitive to SCR variation and mode 1 migrates into the instability as the SCR decreased. This results show how the SCR reduction can greatly affect the system stability. Table II reveals that the DC-Link voltage state has largest participation in mode 1.

C. Influence of voltage control gain change

In order to investigate the influence of changing the voltage controller gain on the system stability Fig. 9 demonstrates the root-locus with voltage controller gain is increased by multiples varying from 1 to 10. From Fig. 9, it is obvious that with the increase in gain from 1 to 10, the stability of the system will be also increased.

TABLE II

Relative Participation Of State Variables In Modes

States	Drive Train			PMSG		MSC		DC	GSC						PLL	
	$\Delta\theta_{tr}$	$\Delta\omega_t$	$\Delta\omega_r$	Δi_{sd}	Δi_{sq}	$\Delta\varphi_3$	$\Delta\varphi_2$	$\Delta\varphi_1$	Δv_{dc}	Δi_{gd}	Δi_{gq}	$\Delta\varphi_7$	$\Delta\varphi_6$	$\Delta\varphi_5$	$\Delta\varphi_4$	$\Delta\varphi_8$	θ_{PLL}
Modes																	
1	0	0	0	0	0	0	0	0	100	66.73	0.191	0.119	0.12	30.23	60.381	0	0.04
2	0	0	0	0	0	0	0	0	0.021	0.427	100	44.44	1.86	0.256	0.067	0	0.028
3	0	0	0	0	0	0	0	0	6.485	100	0.702	0.406	0.03	56.58	82.254	0	0.007
4	0	0	0	0	0	0	0	0	0.944	12.53	0.002	0.014	0	100	2.134	0	0.001
5	0	0	0	0	0	0	0	0	0	0.014	46.572	100	0.52	0.021	0	0	0.001
6	0	0	0	0	0	0	0	0	0.004	0.005	0.143	0.014	0.15	0	0.004	100	100
7	0	0	0	0	0	0	0	0	0.001	0.137	0.131	2.787	100	0	0.001	0.01	0.005
8	15.42	0.494	61.1	0	100	0	80.5	1.43	0	0	0	0	0	0	0	0	0
9	0	0	0	100	0	100	0	0	0	0	0	0	0	0	0	0	0
10	100	13.691	78.7	0	30.92	0	33.5	5.003	0	0	0	0	0	0	0	0	0
11	3.084	90.404	12.7	0	0.155	0	0.14	100	0	0	0	0	0	0	0	0	0

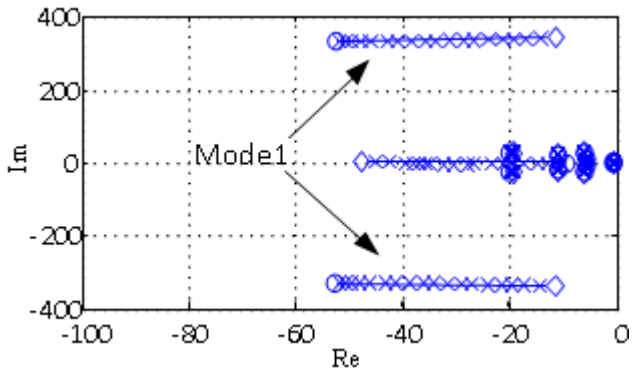

Fig. 8. Linearized model modes loci when varying the SCR(from 10 to 1) .

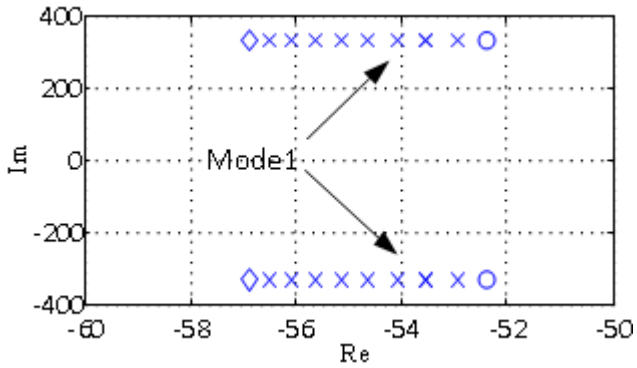

Fig. 9. Root-locus of mode 1 with variation of voltage controller gains (SCR = 10).

IV. ONLINE GRID IMPEDANCE ESTIMATION USING EKF

This section focuses on the Extended Kalman Filter algorithm basics and elaborates the proposed EKF strategy for grid impedance estimation.

A. EKF Algorithm for Parameter Estimation

The Extended Kalman Filter is an optimal estimator for estimating the states of dynamic nonlinear systems [14]. In order to understand the usage of EKF for parameter estimation , the state-space model for a linear system given by equations (39, 40) is considered.

$$x_1(k+1) = A_{1d}x_1(k) + B_{1d}u_1(k) + \varepsilon(k) \tag{39}$$

$$y_1(k) = C_{1d}x_1(k) + v(k) \tag{40}$$

where x_1, u_1 *and* y_1 are state, input and output vectors. The system is subjected to process noise ε and measurement noise$v$. A_{1d}, B_{1d} *and* C_{1d} are the state , input and the output matrices respectively. These matrices are linear time invariant provided that the system parameters are constant.

In order to use EKF for parameter estimation, all system variable parameters summed in parameter vector $\emptyset$ are treated as system states [8]. Adding this parameters vector to the system will cause the system equations to be nonlinear as given by (41,42).

$$\begin{bmatrix} x_1(k+1) \\ \emptyset(k+1) \end{bmatrix} = f(x_1(k), u_1(k), \emptyset(k)) + 1)) + \begin{bmatrix} \varepsilon_x(k) \\ \varepsilon_\emptyset(k) \end{bmatrix} \tag{41}$$

$$y_1(k) = C_{1d}x_1(k) + v(k) \tag{42}$$

where ε_x *and* $\varepsilon_\emptyset$ are state and parameter related noise respectively.

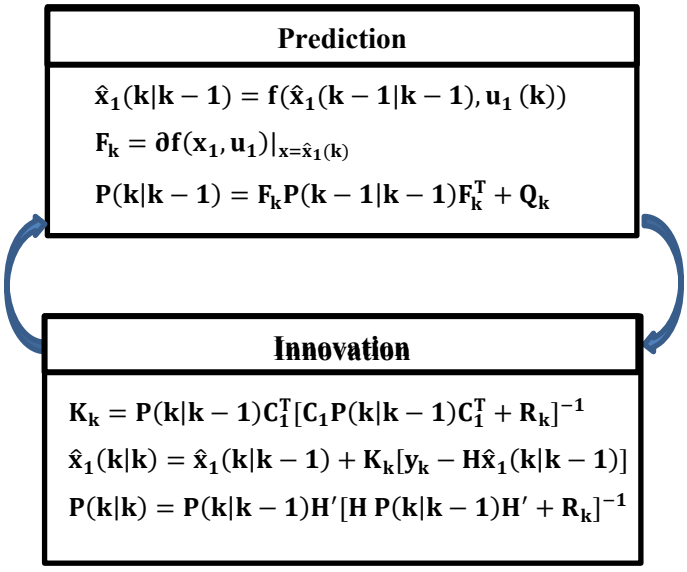

Fig. 10. Extended Kalman-Filter algorithm for parameter estimation.

Figure 10 explains the necessary steps that should be done for implementing the EKF algorithm for parameter estimation based on [14]. The two main parts of the algorithm are the prediction and the innovation steps. In the prediction step, the system states including the parameters are estimated based on the system model and the error-covariance matrix P_k is estimated. The innovation step makes the necessary correction for the predicted states using actual system measurements and the Kalman gain is calculated. At last the updated value of the error-covariance matrix is calculated to be used in the following prediction step. Q_k and R_k are the process noise and measurement covariance matrices.

B. Grid Impedance Estimation Model

The grid can be modeled using the state space representation in (43).

$$\frac{d}{dt}\begin{bmatrix} i_{gd} \\ i_{gq} \end{bmatrix} = -\omega_b \begin{bmatrix} \frac{R_g}{L_g} & -1 \\ 1 & \frac{R_g}{L_g} \end{bmatrix} \begin{bmatrix} i_{gd} \\ i_{qd} \end{bmatrix} + \frac{\omega_b}{L_g}\begin{bmatrix} 1 & 0 & -1 & 0 \\ 0 & 1 & 0 & -1 \end{bmatrix} \begin{bmatrix} v_{gd} \\ v_{gq} \\ v_{pccd} \\ v_{pccq} \end{bmatrix} \tag{43}$$

In order to obtain the grid impedance using the EKF algorithm, the proposed model is reformulated to include both grid voltage and measured PCC voltages in the state vector as in (44) based on [8]. A disturbance observer formulation is

obtained with the advantage of including measurement noise from both voltage and current-measurements into the EKF algorithm. The system measurement is introduced by (45).

$$\frac{d}{dt}\begin{bmatrix} i_{gd} \\ i_{gq} \\ v_{pccd} \\ v_{pccq} \\ v_{gd} \\ v_{gq} \end{bmatrix} = \underbrace{\begin{bmatrix} -\frac{R_g}{L_g} & 0 & -\frac{1}{L_g} & 0 & \frac{1}{L_g} & 0 \\ 0 & -\frac{R_g}{L_g} & 0 & -\frac{1}{L_g} & 0 & \frac{1}{L_g} \\ 0 & 0 & 0 & 0 & 0 & 0 \\ 0 & 0 & 0 & 0 & 0 & 0 \\ 0 & 0 & 0 & 0 & 0 & 0 \\ 0 & 0 & 0 & 0 & 0 & 0 \end{bmatrix}}_{A_1} \begin{bmatrix} i_{gd} \\ i_{gq} \\ v_{pccd} \\ v_{pccq} \\ v_{gd} \\ v_{gq} \end{bmatrix} \quad (44)$$

$$y = \begin{bmatrix} i_{gd} \\ i_{gq} \\ v_{pccd} \\ v_{pccq} \end{bmatrix} = \underbrace{\begin{bmatrix} 1 & 0 & 0 & 0 & 0 & 0 \\ 0 & 1 & 0 & 0 & 0 & 0 \\ 0 & 0 & 1 & 0 & 0 & 0 \\ 0 & 0 & 0 & 1 & 0 & 0 \end{bmatrix}}_{C_1} \begin{bmatrix} i_{gd} \\ i_{gq} \\ v_{pccd} \\ v_{pccq} \\ v_{gd} \\ v_{gq} \end{bmatrix} \quad (45)$$

In order to implement the EKF algorithm in discrete time domain, the transformation shown in (46, 47) is used. Finally, the state vector is extended to include the grid parameters (L_g, R_g) in order to obtain the final formulation presented in (48).

$$A_{1d} = e^{A_1 T} \quad (46)$$

$$C_{1d} = C_1 \quad (47)$$

Simulations under different grid impedance are conducted to show the EKF algorithm ability to estimate the grid parameters. The simulations are introduced in the results section.

C. Proposed GSC Adaptive Controller

In this paper an adaptive control strategy depending on gain scheduling is adopted. Gain-Scheduling is the simplest adaptive control scheme in which the controller parameters are obtained from a pre-determined relation or a look-up table whose values depend on plant variables measurement. The participation factor studies held in section III shows that the critical system modes at low SCR are associated with GSC states. The sensitivity analysis showed that as the voltage controller gain increases, the critical system modes becomes more stable. The proposed method ensures more stability limit under weak grid conditions by adjusting the voltage controller gain constantly according to the current grid impedance estimation obtained from the EKF. Different scheduling techniques are proposed in literature. In [4], the voltage controller gain is scheduled according to simple direct relation between the gain and estimated grid inductance and resistance. In [3], the gain is scheduled using a relation that varies according to the SCR range. In this paper, scheduling relation is given by (50). Figure 11 shows the integration between the grid impedance estimation algorithm and adaptive controller to enhance the system stability.

$$k_{p6} = k_{p6o} * k_s * \sqrt{{R_g}^2 + {X_g}^2} \quad (50)$$

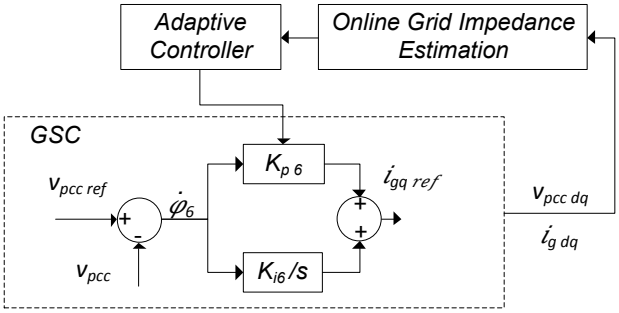

Fig. 11. Proposed adaptive control structure.

V. Simulation Results

In order to verify the effectiveness of the proposed adaptive controller, simulation of the 1.5 MW type IV wind turbine is carried out. A typical grid connection structure is applied, as shown in Fig. 1. The impedance of the grid is varied to simulate different grid weakness levels.

A. Online Grid Impedance Estimation Algorithm Validation

In this section the proposed EKF-based grid impedance estimation algorithm is verified. In order to test the proposed algorithm the SCR of the grid is varied as steps from SCR=3 to SCR=2 with (X/R) ratio kept constant at 10 .The estimated parameters (R_g, L_g) are compared with their actual values in p.u. as shown in Fig.12. The comparison shows the accuracy of the proposed algorithm with low steady state error and satisfactory settling time.

$$\underbrace{\begin{bmatrix} i_{gd}(k+1) \\ i_{gq}(k+1) \\ v_{pccd}(k+1) \\ v_{pccq}(k+1) \\ v_{gd}(k+1) \\ v_{gq}(k+1) \\ R_g(k+1) \\ L_g(k+1) \end{bmatrix}}_{x_1(k)} = \underbrace{\begin{bmatrix} \left(1-\propto \frac{R_g(k)}{L_g(k)}\right) i_{gd}(k) + \propto i_{gq}(k) - \left(\frac{\propto}{L_g(k)}\right) v_{pccd}(k) + \left(\frac{\propto}{L_g(k)}\right) v_{gd}(k) \\ -\propto i_{gd}(k) + \left(1-\propto \frac{R_g(k)}{L_g(k)}\right) i_{gq}(k) - \left(\frac{\propto}{L_g(k)}\right) v_{pccq}(k) + \left(\frac{\propto}{L_g(k)}\right) v_{gq}(k) \\ v_{pccd}(k) \\ v_{pccq}(k) \\ v_{gd}(k) \\ v_{gq}(k) \\ R_g(k) \\ L_g(k) \end{bmatrix}}_{f(x_1(k))} + \varepsilon(k) \quad (48)$$

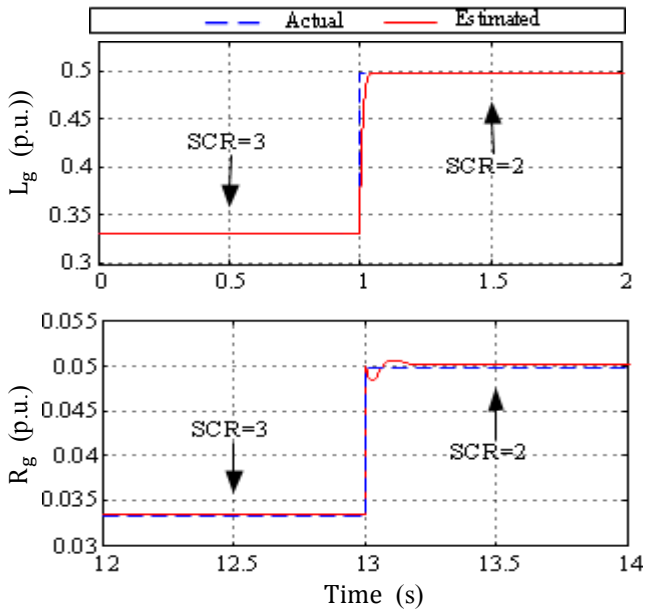

Fig. 12. Online grid impedance estimation algorithm validation .

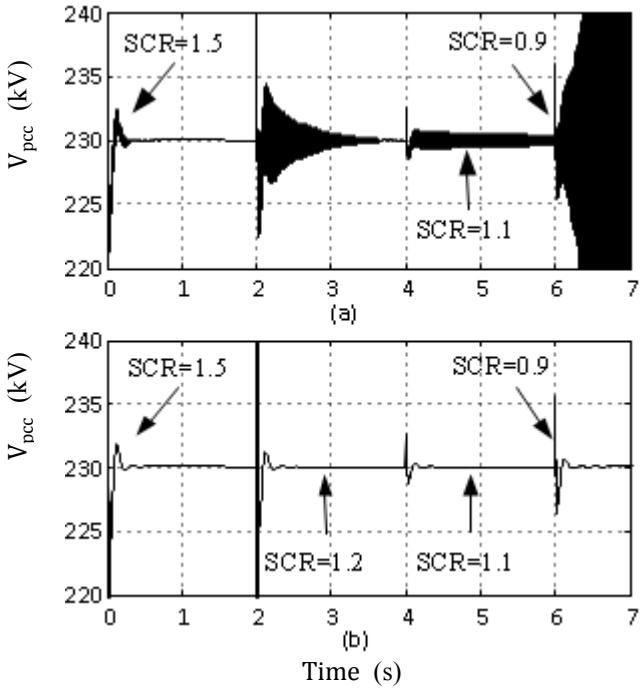

Fig. 13. PCC Voltage under weak grid conditions: (a) Response without adaptive control and (b) Response with adaptive control .

B. Adaptive Controller Effect

The behavior of the proposed system under weak grid conditions without applying the adaptive controller is shown in Fig. 13a while varying SCR from (1.5 to 0.9) which represent very weak grid conditions. As the SCR decreases the damping of the oscillations in PCC voltage is decreased until the system becomes clearly unstable at SCR=0.9. These time domain simulation results matching the results from the eigenvalue analysis which states that the system critical mode migrates to instability at low SCRs. In order to verify the proposed adaptive schemes the same weak grid conditions are used. Fig. 13b shows the behavior of the system after applying the proposed adaptive scheme by modifying the PCC voltage control loop gains according to the estimated grid parameters using the EKF. It can be shown that PCC voltage is quite well damped at very low SCRs.

VI. Conclusion

In this paper, the stability of type IV wind turbine is investigated under weak grid conditions. Initially the small signal model of the utilized PMSG wind turbine generator is presented. The model is then validated against time domain simulations adopted by MATLAB/Simulink. Sensitivity analysis is conducted to reveal the system critical modes under the low grid strength. An online grid impedance estimation using Extended Kalman-Filter approach is introduced. Gain scheduling based adaptive controller is proposed for enhancing GSC stability under weak grid conditions. Simulation results verify the efficiency of the proposed approach.

References

[1] T. Ackermann, Wind Power in Power Systems. Chichester, U.K.: Wiley, 2005.

[2] N. P. W. Strachan and D. Jovcic, "Stability of a variable-speed permanent magnet wind generator with weak AC Grids," IEEE Transactions on Power Delivery, vol. 25, no. 4, pp. 2779–2788, 2010.

[3] L.-J. Cai and I. Erlich, "Doubly Fed Induction Generator Controller Design for the Stable Operation in Weak Grids," *IEEE Transactions on Sustainable Energy*, vol. 6, no. 3, pp. 1078–1084, 2015.

[4] S. Abulanwar, W. Hu, F. Iov, and Z. Chen, "Adaptive voltage control strategy for variable-speed wind turbine connected to a weak network," *IET Renewable Power Generation*, vol. 10, no. 2, pp. 238–249,. 2016.

[5] S. Cobreces, E. J. Bueno, D. Pizarro, F. J. Rodriguez, and F. Huerta, "Grid Impedance Monitoring System for Distributed Power Generation Electronic Interfaces," Instrumentation and Measurement, IEEE Transactions on, vol. 58, no. 9, pp. 3112-3121, Sept.2009.

[6] L. Asiminoaei, R. Teodorescu, F. Blaabjerg, and U. Borup, "Implementation and Test of an Online Embedded Grid Impedance Estimation Technique for PV Inverters," Industrial Electronics, IEEE Transactions on, vol. 52, no. 4, pp. 1136-1144, Aug.2005.

[7] M. Ciobotaru, R. Teodorescu, P. Rodriguez, A. Timbus, and F. Blaabjerg, "Online grid impedance estimation for single-phase grid-Connected connected systems using PQ variations," in Proc. Power Electronics Specialists Conference, 2007. PESC 2007. IEEE, 2007.

[8] N Hoffmann, FW Fuchs," Online grid impedance estimation for the control of grid connected converters in inductive-resistive distributed power-networks using extended kalman-filter", Energy Conversion Congress and Exposition (ECCE), 2012 IEEE, 922-929.

[9] J. Su, L. Shi, L. Yao, Y. Ni, and Z. Guo, "A comparative sub-synchronous resonance analysis of grid-connected doubly fed induction generator based and permanent magnet synchronous generator based wind farms," Electric Power Components and Systems, vol. 43, no. 7, pp. 792–809, Apr. 2015.

[10] M. Chinchilla, S. Arnaltes, and J. C. Burgos, "Control of permanent-magnet generators applied to variable-speed wind-energy systems connected to the grid," IEEE Trans. Energy Convers., vol. 21, no. 1, pp. 130–135, Mar. 2006.

[11] A. Yazdani and R. Iravani, Voltage-sourced converters in power systems: Modeling, control, and applications. United States: IEEE Press/John Wiley, 2010.

[12] D. Hiranya Ravipriya, Sub-synchronous Interactions in a Wind Integrated Power System, PhD thesis, University of Manitoba, Canada, 2014.

[13] C. E. Ugalde-Loo, J. B. Ekanayake, and N. Jenkins, "State-space modeling of wind turbine generators for power system studies," IEEE Transactions on Industry Applications, vol. 49, no. 1, pp. 223–232, Jan. 2013.

[14] G. Welch and G. Bishop, "An Introduction to the Kalman Filter," Tech. Rep. SIGGRAPH 2001 Course at University of North Carolina at Chapel Hill, 2004.